INTERNATIONAL JOURNAL FOR NUMERICAL METHODS IN FLUIDS, VOL. 20, 115–133 (1995)

A SEMI-IMPLICIT LAGRANGIAN SCHEME FOR 3D SHALLOW WATER FLOW WITH A TWO-LAYER TURBULENCE MODEL

PETER K. STANSBY AND PETER M. LLOYD

Hydrodynamics Research Group, Department of Engineering, Simon Building, University of Manchester, Manchester M13 9PL, U.K.

SUMMARY

A semi-implicit Lagrangian finite difference scheme for 3D shallow water flow has been developed to include an eddy viscosity model for turbulent mixing in the vertical direction. The σ-co-ordinate system for the vertical direction has been introduced to give accurate definition of bed and surface boundary conditions. The simple two-layer mixing length model for rough surfaces is used with the standard assumption that the shear stress across the wall region at a given horizontal location is constant. The bed condition is thus defined only by its roughness height (avoiding the need for a friction formula relating to depth-averaged flow, e.g. Chezy, used previously). The method is shown to be efficient and stable with an explicit Lagrangian formulation for convective terms and terms for surface elevation and vertical mixing handled implicitly. The method is applied to current flow around a circular island with gently sloping sides which produce periodic recirculation zones (vortex shedding). Comparisons are made with experimental measurements of velocity using laser Doppler anemometry (time histories at specific points) and surface particle-tracking velocimetry.

KEY WORDS Shallow water flow Turbulence

INTRODUCTION

Computational schemes for the simulation of the shallow water equations in depth-averaged form have become widely used following the pioneering work of Leendertse.[1] He used an alternating direction implicit (ADI) time-stepping scheme for the equations in non-conservation form with finite difference spatial discretization. Explicit schemes have since been used for the equations in conservation form with finite difference[2] and finite element[3] discretization. Rectangular[2] and boundary-fitted[3,4] meshes have been used. The latter ideally requires remeshing at each time step if the wet/dry boundaries are moving, although to date this has not been attempted to our knowledge. The methods above are Eulerian, i.e. the equations are solved in partial differential form (with flow properties only required at fixed positions). In many cases numerical instability from the convective terms is suppressed by upwind differencing (for implicit as well as explicit schemes). This inevitably introduces numerical diffusion and loss of accuracy, although the technique has become more sophisticated over the years.[5,6] (The references given above are a selection familiar to the authors and many more are given in the wide-ranging review of the ASCE.[7])

Recently a Lagrangian scheme for convective terms has been introduced.[8] Here (to first order in time) a fluid particle is assumed to arrive at a mesh point at the end of a time step and its

CCC 0271–2091/95/020115–19

Received January 1994
Revised August 1994

known velocity at the beginning of the time step is assumed constant over the time step and equal to that at the mesh point. The position of the particle at the beginning of the time step may thus be obtained and its velocity obtained through interpolation from the values at the surrounding mesh points. The total derivative for velocity may thus be introduced into the numerical scheme. The method is explicit but does not have the time step limitation of Eulerian schemes (the Courant condition). The experience of Casulli[8] and the present authors is that the technique is stable and accurate. Upwind differencing is avoided. The method may readily be made higher-order in time. (There is corresponding experience for vortex methods which are Lagrangian.[9]) The water surface elevation gradient and a linearized form of the bed shear stress terms are treated implicitly for stability and the horizontal diffusion terms explicitly. The numerical scheme fully coupled in two orthogonal directions gives a five-diagonal equation set. With modern numerical algorithms based on the preconditioned conjugate gradient method such equation sets may be solved very efficiently particularly on a vector processor. The Lagrangian part of the code also vectorized readily and overall such an approach is well suited to modern computing. (Some results from such a code will be presented in this paper.)

Computations based on the three-dimensional form of the shallow water equations are a more recent development. Pressure is still assumed to be hydrostatic. This implies that the horizontal pressure gradients are independent of vertical position, which is a similar assumption to that inherent in the parabolic form of equations used in certain bounded viscous flow problems.[10] The physical implication is that weak or secondary effects driven by attached boundary layers in the vertical direction are reproduced while gross effects such as flow separation or steep wave evolution are not. The Eulerian ADI system for depth-averaged flows has been extended to three dimensions.[11,12] The horizontal momentum equations are now required for a specified number of vertical levels and substituted into the continuity equation integrated over water depth to give a simultaneous equation set with water surface elevations as unknowns. In Reference 12 the so-called σ-co-ordinate system[13] is used in the vertical direction so that the depth at any horizontal position is divided into the same number of segments (this will be fully described later). The vertical diffusion terms are handled implicitly for stability and the convective terms by a mixture of an implicit scheme with upwind differencing, an explicit scheme with central differencing and some high-order dissipation. The horizontal diffusion terms including only second derivatives of velocity are also handled implicitly. Simple turbulence models have been incorporated with various formulae for bed shear stress.

The semi-implicit Lagrangian scheme has also been extended to three dimensions.[14] The vertical diffusion term is again treated implicitly for stability while the horizontal diffusion terms are treated explicitly. The explicit Lagrangian form for the convective terms is a straightforward development from the depth-averaged case. A constant vertical diffusion coefficient was employed (which may be chosen from empirical considerations) and a simple bed boundary condition was used based on the Chezy formula. A uniform vertical mesh was set up (in real space). An advantage of the uniform vertical mesh suggested by the authors is that for very shallow water (which is often a large part of a computational domain) the equations revert to the depth-averaged equations and the numerical solution is quite efficient. A disadvantage is clearly that the vertical velocity gradients are only roughly approximated at the bed and at the water surface.

In this paper we develop the formulation of Casulli and Cheng[14] because the Lagrangian scheme for the convective terms has desirable characteristics as described above. In order to resolve accurately the vertical velocity gradients, we use the σ-co-ordinate system. We incorporate the well-established two-layer eddy viscosity model for the vertical direction.[15] We use the rough turbulent boundary layer approximation with the result that only the bed roughness height is required to specify bed conditions (thereby avoiding the need for a formula

such as Chezy's). The bed boundary condition is based on the well-established criterion that the shear stress is constant across the law-of-the-wall region. A rectangular horizontal mesh is used. This means that the wet/dry boundary generally crosses the mesh cells obliquely, but since this boundary is moving in time, a boundary-fitted mesh would require generation at each time step. Ideally an adaptive mesh system with new boundaries would be generated at each time step, but this is not attempted here.

Prediction of unsteady recirculating flows is a challenging problem in fluid mechanics[16] and particularly challenging for shallow water flows with many practical implications. In this paper we present results for flow around a circular island with gently sloping sides where vigorous vortex shedding occurs (perhaps surprisingly). Computational results are compared with experimental measurements of velocity variation with time at specific points obtained by laser Doppler anemometry. A surface velocity vector plot is also compared with one obtained by particle-tracking velocimetry (PTV).[17]

MATHEMATICAL FORMULATION

Definitions of water surface elevation η, water depth h and bed elevation z_0 are shown in Figure 1.

Starting from the Navier–Stokes equations and taking mean quantities in an averaging time Δt which is small in relation to the time scales of the large-scale, slowly varying structures in a flow, we obtain the Reynolds equation system. We then accept the Boussinesq assumption relating the turbulent stresses introduced by the averaging process to the mean velocity gradients. Furthermore, in shallow water flows we assume the pressure p to be hydrostatic so that

$$p = \rho g(\eta - z), \tag{1}$$

giving

$$\frac{1}{\rho}\frac{\partial p}{\partial x} = g\frac{\partial \eta}{\partial x}, \qquad \frac{1}{\rho}\frac{\partial p}{\partial y} = g\frac{\partial \eta}{\partial y}, \tag{2}$$

where ρ is the fluid density, g is the gravitational acceleration and (x, y, z) is the orthogonal co-ordinate system.

The equation system with the continuity equation thus becomes (ignoring Coriolis forces)

$$\frac{\partial u}{\partial t} + u\frac{\partial u}{\partial x} + v\frac{\partial u}{\partial y} + w\frac{\partial u}{\partial z} = -g\frac{\partial \eta}{\partial x} + \frac{\mu_H}{\rho}\left(\frac{\partial^2 u}{\partial x^2} + \frac{\partial^2 u}{\partial y^2}\right) + \frac{\partial}{\partial z}\left(\frac{\mu_V}{\rho}\frac{\partial u}{\partial z}\right), \tag{3}$$

$$\frac{\partial v}{\partial t} + u\frac{\partial v}{\partial x} + v\frac{\partial v}{\partial y} + w\frac{\partial v}{\partial z} = -g\frac{\partial \eta}{\partial y} + \frac{\mu_H}{\rho}\left(\frac{\partial^2 v}{\partial x^2} + \frac{\partial^2 v}{\partial y^2}\right) + \frac{\partial}{\partial z}\left(\frac{\mu_V}{\rho}\frac{\partial v}{\partial z}\right), \tag{4}$$

$$\frac{\partial u}{\partial x} + \frac{\partial v}{\partial y} + \frac{\partial w}{\partial z} = 0, \tag{5}$$

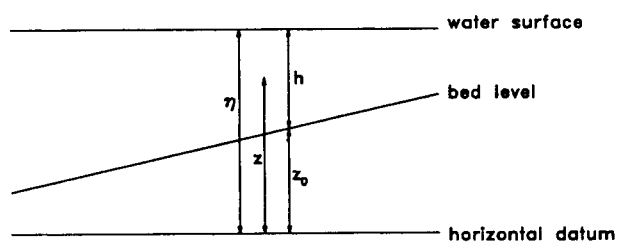

Figure 1. Definition sketch

where u, v and w are the velocities in directions x, y and z respectively, μ_H is the horizontal diffusion coefficient and μ_V is the vertical diffusion coefficient. The continuity equation may be integrated over depth to give

$$\frac{\partial \eta}{\partial t} + \frac{\partial}{\partial x}\int_{z_o}^{\eta} u \, dz + \frac{\partial}{\partial y}\int_{z_o}^{\eta} v \, dz = 0. \tag{6}$$

There are boundary conditions for shear stress at the bed,

$$\mu_V \frac{\partial u}{\partial z} = \tau_x^b, \qquad \mu_V \frac{\partial v}{\partial z} = \tau_y^b, \tag{7}$$

and at the water surface (due to wind),

$$\mu_V \frac{\partial u}{\partial z} = \tau_x^w, \qquad \mu_V \frac{\partial v}{\partial z} = \tau_y^w, \tag{8}$$

Hereafter we ignore any influence of wind, i.e. $\tau_x^w = \tau_y^w = 0$.

We now translate to the σ-co-ordinate system where

$$\sigma = \frac{z - \eta}{h}, \tag{9}$$

giving $\sigma = 0$ when $z = \eta$ and $\sigma = -1$ when $z = z_o$. Since $u = u(x, y, \sigma, t)$,

$$\frac{du}{dt} = \frac{\partial u}{\partial t} + u\frac{\partial u}{\partial x} + v\frac{\partial u}{\partial y} + \frac{d\sigma}{dt}\cdot\frac{\partial u}{\partial \sigma}, \tag{10}$$

with a corresponding expression for dv/dt, and we define $\omega = h\, d\sigma/dt$. Also

$$\frac{\partial}{\partial z}\left(\frac{\mu_V}{\rho}\frac{\partial u}{\partial z}\right) = \frac{\partial \sigma}{\partial z}\cdot\frac{\partial}{\partial \sigma}\left(\frac{\mu_V}{\rho}\frac{\partial u}{\partial \sigma}\cdot\frac{\partial \sigma}{\partial z}\right), \tag{11}$$

with a corresponding expression for

$$\frac{\partial}{\partial z}\left(\frac{\mu_V}{\rho}\cdot\frac{\partial v}{\partial z}\right).$$

Since

$$\frac{\partial \sigma}{\partial z} = \frac{1}{h},$$

the shallow water equations become

$$\frac{\partial u}{\partial t} + u\frac{\partial u}{\partial x} + v\frac{\partial u}{\partial y} + \frac{\omega}{h}\frac{\partial u}{\partial \sigma} = -g\frac{\partial \eta}{\partial x} + \frac{\mu_H}{\rho}\left(\frac{\partial^2 u}{\partial x^2} + \frac{\partial^2 u}{\partial y^2}\right) + \frac{1}{h}\frac{\partial}{\partial \sigma}\left(\frac{\mu_V}{\rho h}\frac{\partial u}{\partial \sigma}\right), \tag{12}$$

$$\frac{\partial v}{\partial t} + u\frac{\partial v}{\partial x} + v\frac{\partial v}{\partial y} + \frac{\omega}{h}\frac{\partial v}{\partial \sigma} = -g\frac{\partial \eta}{\partial y} + \frac{\mu_H}{\rho}\left(\frac{\partial^2 v}{\partial x^2} + \frac{\partial^2 v}{\partial y^2}\right) + \frac{1}{h}\frac{\partial}{\partial \sigma}\left(\frac{\mu_V}{\rho h}\frac{\partial v}{\partial \sigma}\right), \tag{13}$$

The depth-integrated continuity equation is unchanged.

To obtain the vertical velocity ω, we have

$$w = -\int_{z_0}^{z} \left(\frac{\partial u}{\partial x} + \frac{\partial v}{\partial y}\right) h \, d\sigma \quad \text{with} \quad w_{z=z_0} = 0, \tag{14}$$

$$\omega = w - u\left(\sigma \frac{\partial h}{\partial x} + \frac{\partial \eta}{\partial x}\right) - v\left(\sigma \frac{\partial h}{\partial y} + \frac{\partial \eta}{\partial y}\right) - \left(\sigma \frac{\partial h}{\partial t} + \frac{\partial \eta}{\partial t}\right). \tag{15}$$

Note that $\omega = 0$ when $\sigma = 0$ or -1.

The shallow water equations are thus defined in the σ-co-ordinate system.

TURBULENCE MODEL

We incorporate the standard two-layer mixing length model for eddy viscosity[15] describing vertical mixing,

$$\mu_V = \mu + \rho l^2 \left|\frac{\partial u_m}{\partial z}\right|, \tag{16}$$

where $u_m = \sqrt{(u^2 + v^2)}$, μ is the molecular viscosity and l is the mixing length. The two-layer model for l is defined as $l = k(z - z_0)$ for $(z - z_0) < \lambda h/k$ and $l = \lambda h$ for $\lambda h/k < (z - z_0) < h$, where λ and k are turbulent boundary layer constants usually specified as 0·09 and 0·43 respectively. Note here that the local depth h is also the boundary layer thickness. For 'rough' surfaces within the inner or 'wall' region the velocity profile is logarithmic,

$$\frac{u_m}{u_*} = 5{\cdot}75 \log_{10}\left(\frac{B(z - z_0)}{k_s}\right), \tag{17}$$

where $u_* = \sqrt{(\tau^b/\rho)}$ (friction velocity), k_s is the roughness height and B is set conventionally to 33. It is generally accepted that the shear stress within the wall region is constant (for a given horizontal location). For a given vertical position z_1 we thus have

$$\frac{\tau^b}{\rho} = u_*^2 = \frac{u_{m1}^2}{\left[5{\cdot}75 \log_{10}\left(\frac{B(z_1 - z_0)}{k_s}\right)\right]^2}. \tag{18}$$

To give the shear stress components in directions x and y, this expression is conventionally resolved as

$$\tau_x^b = \frac{\rho\sqrt{(u_1^2 + v_1^2)}u_1}{\left[5{\cdot}75 \log_{10}\left(\frac{B(z_1 - z_0)}{k_s}\right)\right]^2} = \gamma u_1, \tag{19}$$

$$\tau_y^b = \frac{\rho\sqrt{(u_1^2 + v_1^2)}v_1}{\left[5{\cdot}75 \log_{10}\left(\frac{B(z_1 - z_0)}{k_s}\right)\right]^2} = \gamma v_1, \tag{20}$$

Equations (7), (19) and (20) together provide the bed boundary condition, i.e. the boundary condition for the cell adjacent to the bed, which should of course lie well within the wall region.

The horizontal diffusion term is of less significance and the empirical expression $\mu_H = \rho c_H u_* h$ is used with $c_H = 0{\cdot}1$. A range of values for c_H has been used[14,18] and 0·1 is chosen as a representative value. μ_H is thus not constant as in Reference 14 and the inclusion of only second-order derivatives in the momentum equations is consistent with Reference 12.

FINITE DIFFERENCE FORMULATION

We use the conventional staggered mesh system with cells numbered i, j, k for directions x, y, z, where $i = 1, \ldots, I, j = 1, \ldots, J$ and $k = 1, \ldots, K$, with $k = 1$ for the bed cell and $k = K$ for the surface cell. The horizontal cell sizes are Δx and Δy. The momentum equations (12) and (13) take the form

$$u^{n+1}_{i+1/2,j,k} = Fu^n_{i+1/2,j,k} - g\frac{\Delta t}{\Delta x}(\eta^{n+1}_{i+1,j} - \eta^{n+1}_{i,j}) + \Delta t \frac{\dfrac{\mu^n_{i+1/2,j,k+1/2}}{\rho}\left(\dfrac{u^{n+1}_{i+1/2,j,k+1} - u^{n+1}_{i+1/2,j,k}}{h^n_{i+1/2,j}\,\mathrm{d}\sigma}\right) - \dfrac{\mu^n_{i+1/2,j,k-1/2}}{\rho}\left(\dfrac{u^{n+1}_{i+1/2,j,k} - u^{n+1}_{i+1/2,j,k-1}}{h^n_{i+1/2,j}\,\mathrm{d}\sigma}\right)}{h^n_{i+1/2,j}\,\mathrm{d}\sigma}, \tag{21}$$

$$v^{n+1}_{i,j+1/2,k} = Fv^n_{i,j+1/2,k} - g\frac{\Delta t}{\Delta y}(\eta^{n+1}_{i,j+1} - \eta^{n+1}_{i,j}) + \Delta t \frac{\dfrac{\mu^n_{i,j+1/2,k+1/2}}{\rho}\left(\dfrac{v^{n+1}_{i,j+1/2,k+1} - v^{n+1}_{i,j+1/2,k}}{h^n_{i,j+1/2}\,\mathrm{d}\sigma}\right) - \dfrac{\mu^n_{i,j+1/2,k-1/2}}{\rho}\left(\dfrac{v^{n+1}_{i,j+1/2,k} - v^{n+1}_{i,j+1/2,k-1}}{h^n_{i,j+1/2}\,\mathrm{d}\sigma}\right)}{h^n_{i,j+1/2}\,\mathrm{d}\sigma}, \tag{22}$$

where n denotes the time level, Δt is the time step and $\mathrm{d}\sigma$ is the vertical mesh spacing, a constant equal to $1/K$ in this case. Note that here the subscript 'V' has been omitted from μ_V to avoid confusion. In more convenient matrix–vector form

$$A^n_{i+1/2,j}U^{n+1}_{i+1/2,j} = G^n_{i+1/2,j} - g\frac{\Delta t}{\Delta x}(\eta^{n+1}_{i+1,j} - \eta^{n+1}_{i,j})h^n_{i+1/2,j}\,\Delta\sigma, \tag{23}$$

$$A^n_{i,j+1/2}V^{n+1}_{i,j+1/2} = G^n_{i,j+1/2} - g\frac{\Delta t}{\Delta y}(\eta^{n+1}_{i,j+1} - \eta^{n+1}_{i,j})h^n_{i,j+1/2}\,\Delta\sigma, \tag{24}$$

where

$$\begin{aligned}
\Delta\sigma &= [1/K, \ldots, 1/K]^T,\\
U^n_{i+1/2,j} &= [u^n_{i+1/2,j,1}, \ldots, u^n_{i+1/2,j,K}]^T,\\
V^n_{i,j+1/2} &= [v^n_{i,j+1/2,1}, \ldots, v^n_{i,j+1/2,K}]^T,\\
G^n_{i+1/2,j} &= \mathrm{d}\sigma\, h^n_{i+1/2,j}[Fu^n_{i+1/2,j,1}, \ldots, Fu^n_{i+1/2,j,K}]^T,\\
G^n_{i,j+1/2} &= \mathrm{d}\sigma\, h^n_{i,j+1/2}[Fv^n_{i,j+1/2,1}, \ldots, Fv^n_{i,j+1/2,K}]^T.
\end{aligned} \tag{25}$$

Here F is the explicit Lagrangian operator described in full below. The tridiagonal matrix A has different forms for directions x and y, though omitting the subscripts '$i + \frac{1}{2}, j$' and

'$i, j + \frac{1}{2}$', it takes the common form

$$A = \begin{bmatrix} (h\,\mathrm{d}\sigma + \gamma\,\Delta t + \Delta t\,\mu_{1\frac{1}{2}}/h\,\mathrm{d}\sigma) & -\Delta t\,\mu_{1\frac{1}{2}}/h\,\mathrm{d}\sigma & & \\ -\Delta t\,\mu_{1\frac{1}{2}}/h\,\mathrm{d}\sigma & (h\,\mathrm{d}\sigma + \Delta t\,\mu_{2\frac{1}{2}}/h\,\mathrm{d}\sigma + \Delta t\,\mu_{1\frac{1}{2}}/h\,\mathrm{d}\sigma) & -\Delta t\,\mu_{2\frac{1}{2}}/h\,\mathrm{d}\sigma & \\ & a_{k-1} \quad a_k \quad a_{k+1} & & \\ & & -\Delta t\,\mu_{K-1/2}/h\,\mathrm{d}\sigma & (h\,\mathrm{d}\sigma + \Delta t\,\mu_{K-1/2}/h\,\mathrm{d}\sigma) \end{bmatrix},$$

where a_{k-1}, a_k and a_{k+1} are the elements of the kth row for $k = 2, \ldots, K-1$ given by

$$a_{k-1} = -\Delta t\,\mu_{k-1/2}/h\,\mathrm{d}\sigma, \quad a_k = h\,\mathrm{d}\sigma + \Delta t\,\mu_{k+1/2}/h\,\mathrm{d}\sigma + \Delta t\,\mu_{k-1/2}/h\,\mathrm{d}\sigma, \quad a_{k+1} = -\Delta t\,\mu_{k+1/2}/h\,\mathrm{d}\sigma. \tag{26}$$

Substituting into the depth-integrated continuity equation gives in matrix notation

$$\eta_{i,j}^{n+1} = \eta_{i,j}^n - \frac{\Delta t}{\Delta x}\left(h_{i+1/2,j}^n\,\Delta\sigma^{\mathrm{T}}\,U_{i+1/2,j}^{n+1} - h_{i-1/2,j}^n\,\Delta\sigma^{\mathrm{T}}\,U_{i-1/2,j}^{n+1}\right)$$
$$- \frac{\Delta t}{\Delta y}\left(h_{i,j+1/2}^n\,\Delta\sigma^{\mathrm{T}}\,V_{i,j+1/2}^{n+1} - h_{i,j-1/2}^n\,\Delta\sigma^{\mathrm{T}}\,V_{i,j-1/2}^{n+1}\right). \tag{27}$$

Substituting for U and V gives

$$\eta_{i,j}^{n+1} - g\,\frac{\Delta t^2}{\Delta x^2}\left[h_{i+1/2,j}^{n^2}\,\Delta\sigma^{\mathrm{T}}A_{i+1/2,j}^{-1}\,\Delta\sigma(\eta_{i+1,j}^{n+1} - \eta_{i,j}^{n+1}) - h_{i-1/2,j}^{n^2}\,\Delta\sigma^{\mathrm{T}}A_{i-1/2,j}^{-1}\,\Delta\sigma(\eta_{i,j}^{n+1} - \eta_{i-1,j}^{n+1})\right]$$
$$- g\,\frac{\Delta t^2}{\Delta y^2}\left[h_{i,j+1/2}^{n^2}\,\Delta\sigma^{\mathrm{T}}A_{i,j+1/2}^{-1}\,\Delta\sigma(\eta_{i,j+1}^{n+1} - \eta_{i,j}^n) - h_{i,j-1/2}^{n^2}\,\Delta\sigma^{\mathrm{T}}A_{i,j-1/2}^{-1}\,\Delta\sigma(\eta_{i,j}^{n+1} - \eta_{i,j-1}^{n+1})\right]$$
$$= \eta_{i,j}^n - \frac{\Delta t}{\Delta x}\left[h_{i+1/2,j}^n\,(\Delta\sigma^{\mathrm{T}}A_{i+1/2,j}^{-1}G_{i+1/2,j})^n - h_{i-1/2,j}^n(\Delta\sigma^{\mathrm{T}}A_{i-1/2,j}^{-1}G_{i-1/2,j})^n\right]$$
$$- \frac{\Delta t}{\Delta y}\left[h_{i,j+1/2}^n(\Delta\sigma^{\mathrm{T}}A_{i,j+1/2}^{-1}G_{i,j+1/2})^n - h_{i,j-1/2}^n(\Delta\sigma^{\mathrm{T}}A_{i,j-1/2}^{-1}G_{i,j-1/2})^n\right], \tag{28}$$

where $\Delta\sigma^{\mathrm{T}}A^{-1}\,\Delta\sigma$ is a positive number. For each point i, j we thus have an equation for $\eta_{i,j}$, $\eta_{i+1,j}$, $\eta_{i,j+1}$, $\eta_{i-1,j}$, $\eta_{i,j-1}$. There are thus $I \times J$ equations which may be solved very efficiently as before using a preconditioned conjugate gradient solver.

Having solved for $\eta_{i,j}$, the vectors U and V may be obtained by solving the tridiagonal equations (23) and (24).

It now remains to solve for $\omega_{i,j,k+1/2}$, $k = 1, \ldots, K$. From continuity we simply have at new time level $n+1$

$$w_{i,j,k+1/2} = w_{i,j,k-1/2} - h_{i,j}\,\mathrm{d}\sigma[(u_{i+1/2,j,k} - u_{i-1/2,j,k})/\Delta x + (v_{i,j+1/2,k} - v_{i,j-1/2,k})/\Delta y]. \tag{29}$$

The corresponding values of $\omega_{i,j,k+1/2}$ are obtained from equation (15) in central difference form as

$$\omega_{i,j,k+1/2} = w_{i,j,k+1/2} - u_{i,j,k+1/2}\left(\sigma_{k+1/2}\frac{h_{i+1,j}-h_{i-1,j}}{2\Delta x} + \frac{\eta_{i+i,j}-\eta_{i-1,j}}{2\Delta x}\right)$$
$$- v_{i,j,k+1/2}\left(\sigma_{k+1/2}\frac{h_{i,j+1}-h_{i,j-1}}{2\Delta y} + \frac{\eta_{i,j+1}-\eta_{i,j-1}}{2\Delta y}\right)$$
$$- \left(\sigma_{k+1/2}\frac{h^{n+1}_{i,j}-h^{n}_{i,j}}{\Delta t} + \frac{\eta^{n+1}_{i,j}-\eta^{n}_{i,j}}{\Delta t}\right). \tag{30}$$

Note that $\sigma_{k+1/2} = -1 + k\,\mathrm{d}\sigma$ and all values are for time level $n+1$ except in the last two terms as indicated.

The method is thus complete apart from the specification of the finite difference operator F. A particle which ends up at a mesh point $i+\frac{1}{2}, j, k$ at the end of a time step has a position at the beginning of the time step which is obtained by assuming that the velocity is constant over the time step. Thus

$$\frac{\mathrm{D}u}{\mathrm{D}t} = \frac{u^{n+1}_{i+1/2,j,k} - u^{n}_{i+1/2-a,j-b,k-c}}{\Delta t}, \tag{31}$$

where

$$a = \frac{u^{n}_{i+1/2,j,k}\,\Delta t}{\Delta x}, \qquad b = \frac{v^{n}_{i+1/2,j,k}\,\Delta t}{\Delta y}, \qquad c = \frac{\omega^{n}_{i+1/2,j,k}\,\Delta t}{h_{i+1/2,j}\,\mathrm{d}\sigma}.$$

The value $u_{i-a,j-b,k-c}$ is found by trilinear interpolation from the eight values on the cell in which the particle is situated.[14] It should be mentioned here that improved estimates for a, b and c may be obtained simply using $\int u^n\,\mathrm{d}t$, $\int v^n\,\mathrm{d}t$ and $\int \omega^n\,\mathrm{d}t$. However, explicit integration using several steps had negligible effect on our results given below.

Including the horizontal diffusion terms explicitly, we now have

$$Fu^{n}_{i+1/2,j,k} = u^{n}_{i+1/2-a,j-b,k-c}$$
$$+ \frac{\mu^{n}_{\mathrm{H}}\,\Delta t}{\rho}\,\frac{u^{n}_{i+1/2-a+1,j-b,k-c} - 2u^{n}_{i+1/2-a,j-b,k-c} + u^{n}_{i+1/2-a-1,j-b,k-c}}{\Delta x^2}$$
$$+ \frac{\mu^{n}_{\mathrm{H}}\,\Delta t}{\rho}\,\frac{u^{n}_{i+1/2-a,j-b+1,k-c} - 2u^{n}_{i+1/2-a,j-b,k-c} + u^{n}_{i-1/2-a,j-b-1,k-c}}{\Delta y^2}, \tag{32}$$

with a corresponding expression for $Fv^{n}_{i,j+1/2,k}$.

It remains to specify the initial and boundary conditions. We are concerned here with subcritical flow; the flow rate is specified at the inlet and the water surface elevation at the outlet. At $t = 0$ the water is stationary and the water level horizontal. The inlet flow rate is increased as a quarter-sinusoid and then maintained at a constant value to represent a steady current. More detailed boundary conditions for the problem to be considered here are given below. To set up the geometry, bed elevations and water surface elevations are input. The wet/dry boundaries are simply handled. If at a (horizontal) velocity mesh point the water depth is less than some small value, set to 0·001 m for these computations, all velocities (u, v, w) at that point are set to zero. If, with lowering water level, the depth at a mesh point becomes less than this small value, all velocities at that point are also set to zero. If, with rising water level, the depth

at a mesh point becomes greater than this small value, it is given a surface elevation with the same horizontal level as an adjacent wet cell and its velocities remain zero but are advanced at the following time step. Setting these velocities through interpolation from adjacent (wet) mesh points was also used but was found to make negligible difference and was regarded as an unnecessary complication.

Varying the cut-off depth for wet/dry boundaries was tested in the depth-averaged computations by increasing it from 1 to 5 mm and this was found to have negligible effect.

APPLICATION TO FLOW AROUND A CONICAL ISLAND

This geometry was chosen so that computational results may be compared with those from an ongoing experimental investigation in a purpose-built 'wide' flume. In the particular case for comparison the water depth is 0·08 m, the mean velocity is 0·088 m s^{-1}, the island side slope is 22° (to the horizontal) and its radius at the intersection with the water surface is 0·07 m. The flume is 1·52 m wide by 5·00 m long and is made of painted marine ply. Without the island present the water depth was virtually constant over the area of the flume (equal to the normal depth). It was not possible to measure the very small bed slope accurately. However, assuming Manning's number to be 0·01 for such a surface gives a bed slope of 0·00002246. This does of course assume a rough turbulent boundary layer which is not ensured for these laboratory conditions, but it does provide a reasonable basis for comparison. In order to determine the corresponding surface roughness height k_s (for the 3D computations), we use the approximate relationship

$$\frac{\bar{u}}{u_*} = 5{\cdot}75 \log\left(\frac{12{\cdot}1\,h}{k_s}\right), \tag{33}$$

where $\bar{u}$ is the mean velocity. For the conditions specified, $k_s = 0{\cdot}000219$ m.

Initial tests were made to check that the water depth attained the normal depth after the transient start from still water conditions (for both 2D and 3D computations). This does not of course indicate the effectiveness of the schemes in simulating transient flows, particularly highly transient flows. An extreme example of the latter is the dam break problem which produces a moving shock and for which there is an analytical solution with the depth-averaged approximation. The numerical method gives effectively exact predictions with subcritical flow behind the shock and nearly exact predictions with supercritical flow behind the shock. A detailed analysis will be given in a separate paper. We are thus satisfied that the computations accurately reproduce viscous effects and highly transient effects in well-established simple test cases (with subcritical flow for the latter).

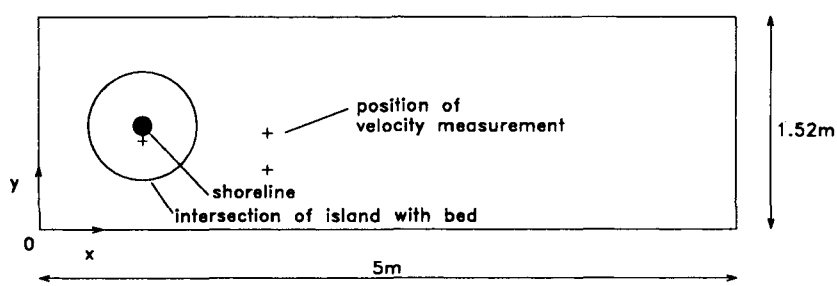

Figure 2. Plan view of island showing co-ordinate system

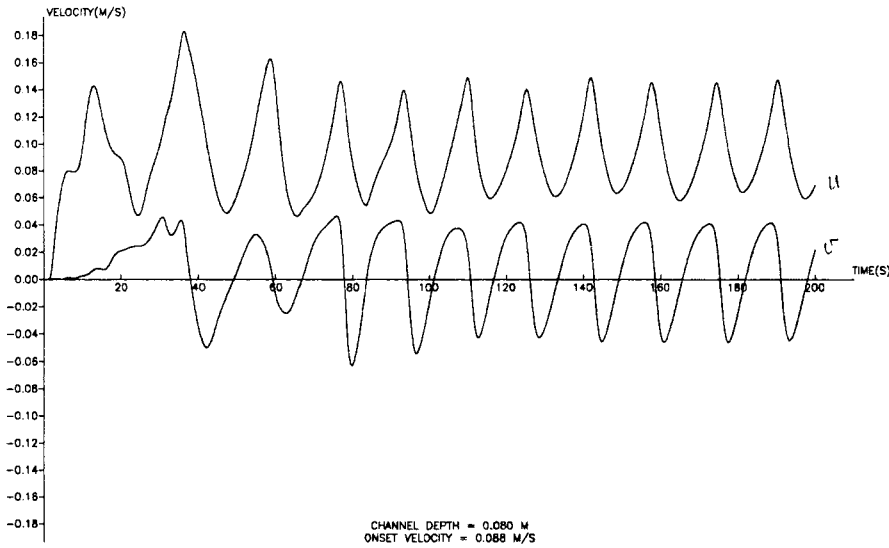

Figure 3. Variation in velocities u and v with time at $x = 1{\cdot}617$ m, $y = 0{\cdot}445$ m from depth-averaged computation; cell size of 0·0152 m, 328 × 100 mesh

Some preliminary 2D computations were made with the island in position to determine appropriate mesh sizes and time step. The numerical scheme is the same as Casulli's apart from the use of Manning's rather than Chezy's formula. A computational domain was set up to correspond to the dimensions of the flume with x and y measured from the bottom left-hand corner in the downstream and cross-stream directions respectively as shown in Figure 2. In these computations the flow remains symmetric for a long time before vortex shedding starts. In order to promote asymmetry, a cross-velocity v at the inlet is superimposed on the

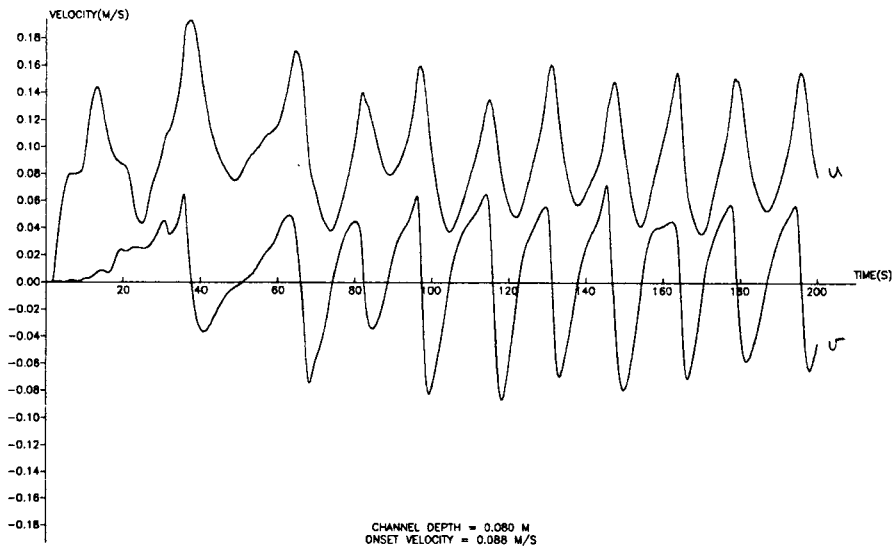

Figure 4. As Figure 3 with a cell size of 0·0076 m, 656 × 200 mesh

longitudinal velocity u such that

$$u = u_0 \sin(2\pi t/T) \quad \text{for } t < T/4\,(=5\text{ s}),$$
$$v = (u/4)[1 - \cos(2\pi t/T_0)][1 - \cos(2\pi y/L)] \quad \text{for } t < T_0, \tag{34}$$

where $T_0 = T/4$ and L is the width of the flume. In this way $v = 0$ at the sides of the flume, a necessary boundary condition. At the outlet boundary $\partial u/\partial x$ and $\partial v/\partial x$ are set to zero (the depth is of course fixed) and at the side walls v, $\partial u/\partial y$ and $\partial \eta/\partial y$ are set to zero. While such simple outflow boundary conditions have been widely used, their limitations are obvious. Their effect on the results is assessed below. Computational domains have been set up using square cells of sizes 0·0304, 0·0152 and 0·0076 m with meshes of 164 × 50, 328 × 100 and 656 × 200 respectively. Time steps of 0·075, 0·05 and 0·025 s were tested with the coarsest mesh and almost identical results (velocity time histories at various positions) were produced for the two smaller values. Results with the 328 × 100 mesh were also almost identical with time steps of 0·025 and 0·05 s. Although the time stepping is only first-order-accurate, a value of 0·05 s appears small enough to give accurate results. On the other hand, the effect of decreasing cell size is more pronounced. Velocity time histories are shown in Figure 3 with a cell size of 0·0152 m and in Figure 4 with a cell size of 0·0076 m at a downstream position for which experimental data are available, namely 0·857 m downstream of the island centre and 0·315 m across from the flume centreline ($x = 1{\cdot}617$ m, $y = 0{\cdot}445$ m). The behaviour is very close for the initial 40 s; differences then appear as vortex shedding becomes established. While the frequencies of velocity fluctuation for regular vortex shedding are almost identical in the two cases, the magnitudes of the fluctuations are noticeably greater for the smaller cell size. This leaves the matter of numerical convergence unresolved, but it appears that a cell size of 0·0152 m is adequate for the qualitative simulation of prominent vortex-shedding characteristics.

The influence of the downstream boundary condition was tested using this cell size and a 528 × 100 mesh (doubling the distance of the outlet boundary from the island centre). The corresponding velocity time history is shown in Figure 5. Since the depth is fixed at the outlet,

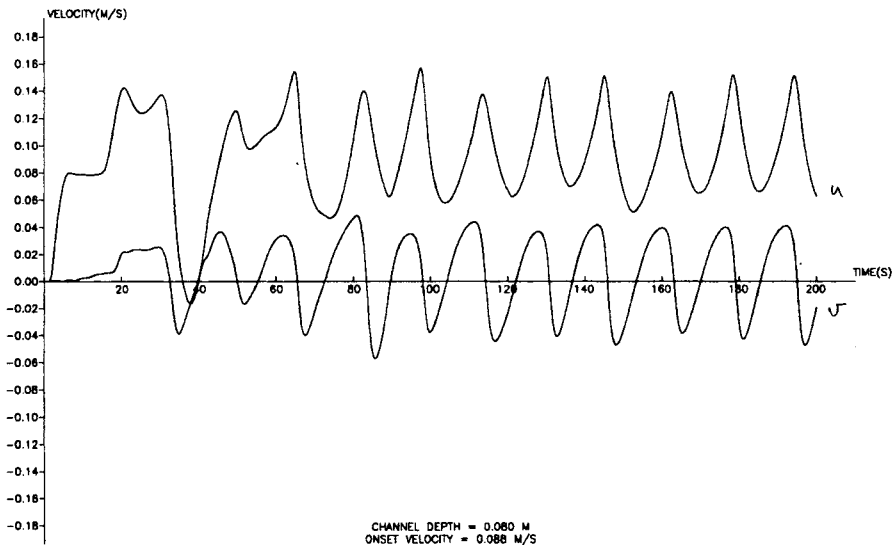

Figure 5. As Figure 3 with a cell size of 0·0152 m, 528 × 100 mesh

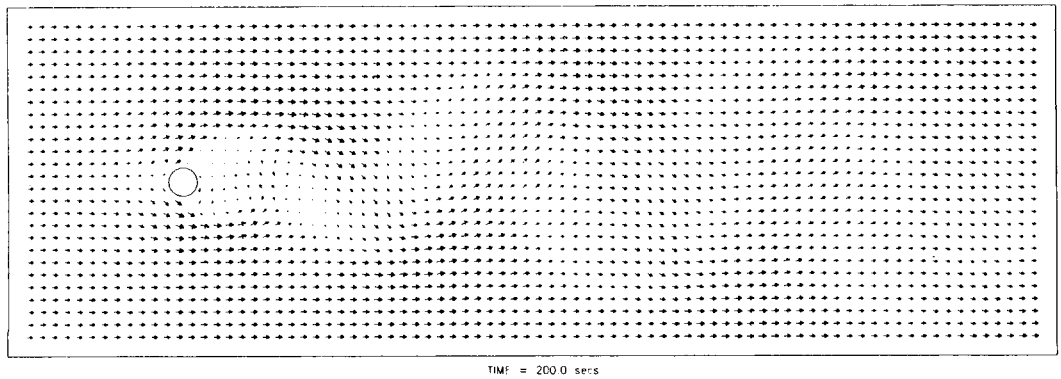

Figure 6. Velocity vector plot at the water surface from 3D computation with a cell size of 0·0152 m, 328 × 100 × 20 mesh (arrow length is proportional to velocity magnitude)

the water depth at the inlet is greater than in the previous tests and a different initial behaviour is thus expected, but the velocity characteristics are very similar once vortex shedding has started (and the depth is fluctuating about the normal depth). This indicates insensitivity of the resulting flow to the simple downstream boundary condition used.

The 3D computations were made with the 0·015 m cell size with 20 vertical divisions (a 328 × 100 × 20 mesh) and a time step of 0·05 s. The inlet and outlet boundary conditions are essentially the same as those described for the 2D computations. At the inlet the velocities u and v are prescribed uniformly over depth with magnitudes given in equation (34) and vertical velocity $w = 0$. At the outlet $\partial u/\partial x$, $\partial v/\partial x$ and $\partial \omega/\partial x$ are now set to zero (across the depth) and at the side walls v, $\partial u/\partial y$ and $\partial \omega/\partial y$ are set to zero (across the depth); $\partial \eta/\partial y$ is also set to zero. A typical velocity vector plot (at the water surface) shows the oscillatory wake structure in Figure 6. Figure 7 shows velocity time histories at bed, mid-depth and surface cells for the same position

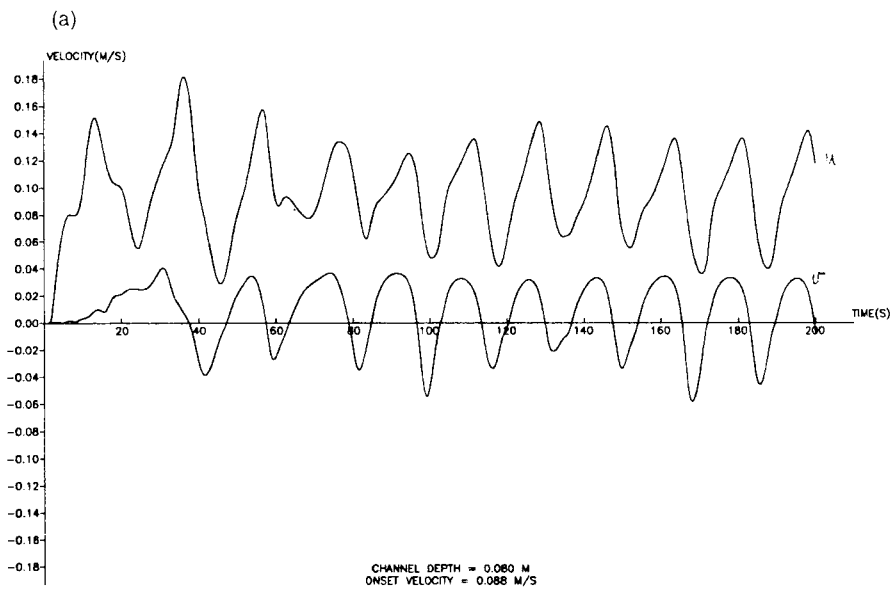

Figure 7. Variation in velocities u and v with time at $x = 1{\cdot}617$ m, $y = 0{\cdot}445$ m from 3D computation; cell size of 0·0152 m, 328 × 100 × 20 mesh: (a) surface cell; (b) mid-depth cell; (c) bed cell

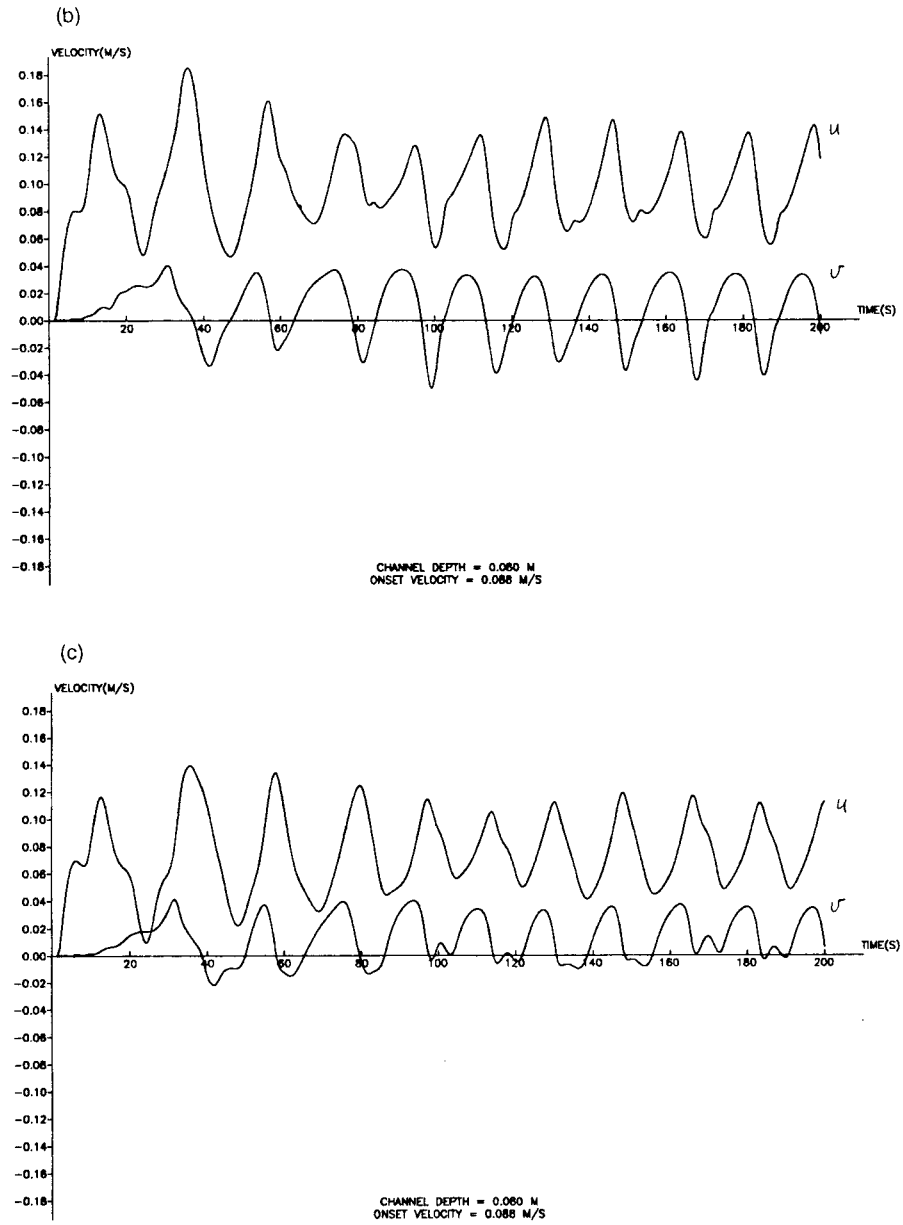

Figure 7. (Continued)

as above. There is little difference between the surface and mid-depth cells, but the bed cell shows different frequency content as well as magnitudes. Figure 8 shows a comparison with experimental measurements of the u-velocity component obtained by laser Doppler anemometry (LDA) for a position about 5 mm below the water surface. There is close agreement in the dominant frequency between experiment and computation and in this case the velocity fluctuations are of similar magnitude, although experimental measurements over longer times are clearly desirable. Surface velocity vector plots have also been obtained experimentally by video analysis of small particles floating in a nearly submerged state (particle-tracking velocimetry[17]). An example is

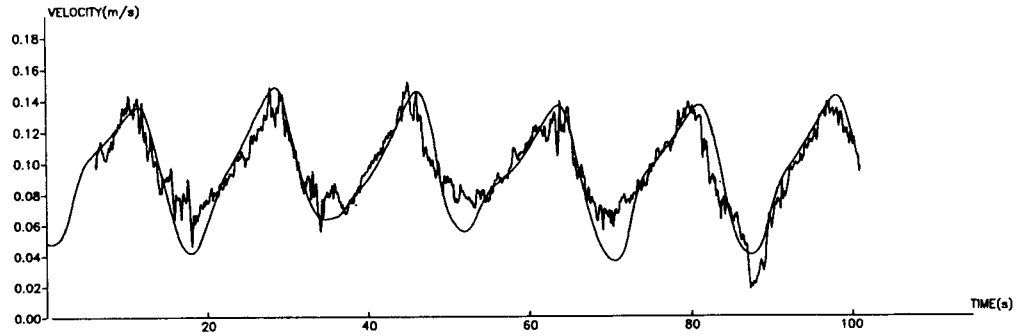

Figure 8. Variation in surface u-velocity with time from computation and LDA experimental measurement at $x = 1{\cdot}617$ m, $y = 0{\cdot}445$ m, the smooth variation being for the former and the spiky variation for the latter

shown in Figure 9(a) which may be compared with that obtained computationally at a corresponding phase in the wake oscillation cycle, shown in Figure 9(b), an enlarged portion of Figure 6. The flow patterns are qualitatively similar.

Experimental measurements were also made at the same downstream distance at 0·034 m from the flume centreline ($x = 1{\cdot}617$ m, $y = 0{\cdot}726$ m). Velocities from the 3D computation are shown in Figure 10 and the u-velocity at the surface is compared with LDA measurements in Figure 11. The experimental measurements here show some marked differences from the computed velocities, the experimental values showing greater irregularity and a different mean

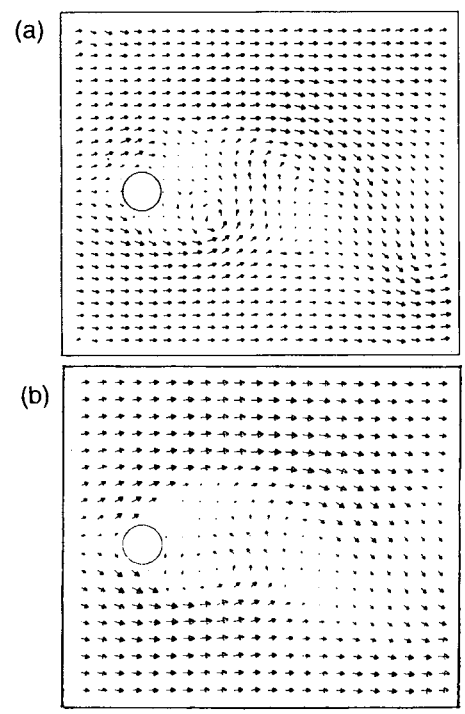

Figure 9. Velocity vector plot at the water surface at $t = 200$ s: (a) obtained in experiment using PTV; (b) obtained computationally, enlarged from Figure 6 for comparison

value. In making comparisons with experiment, however, it must be remembered that numerical convergence in relation to cell size has not been demonstrated and that a rather simple turbulence model has been used. The u-velocity has a dominant frequency of twice that for the v-velocity which corresponds to that at the greater distance from the flume centreline. In this position the computed velocities at bed, mid-depth and surface levels show greater differences. While the v-velocity has a dominant frequency at the second harmonic of the vortex-shedding frequency

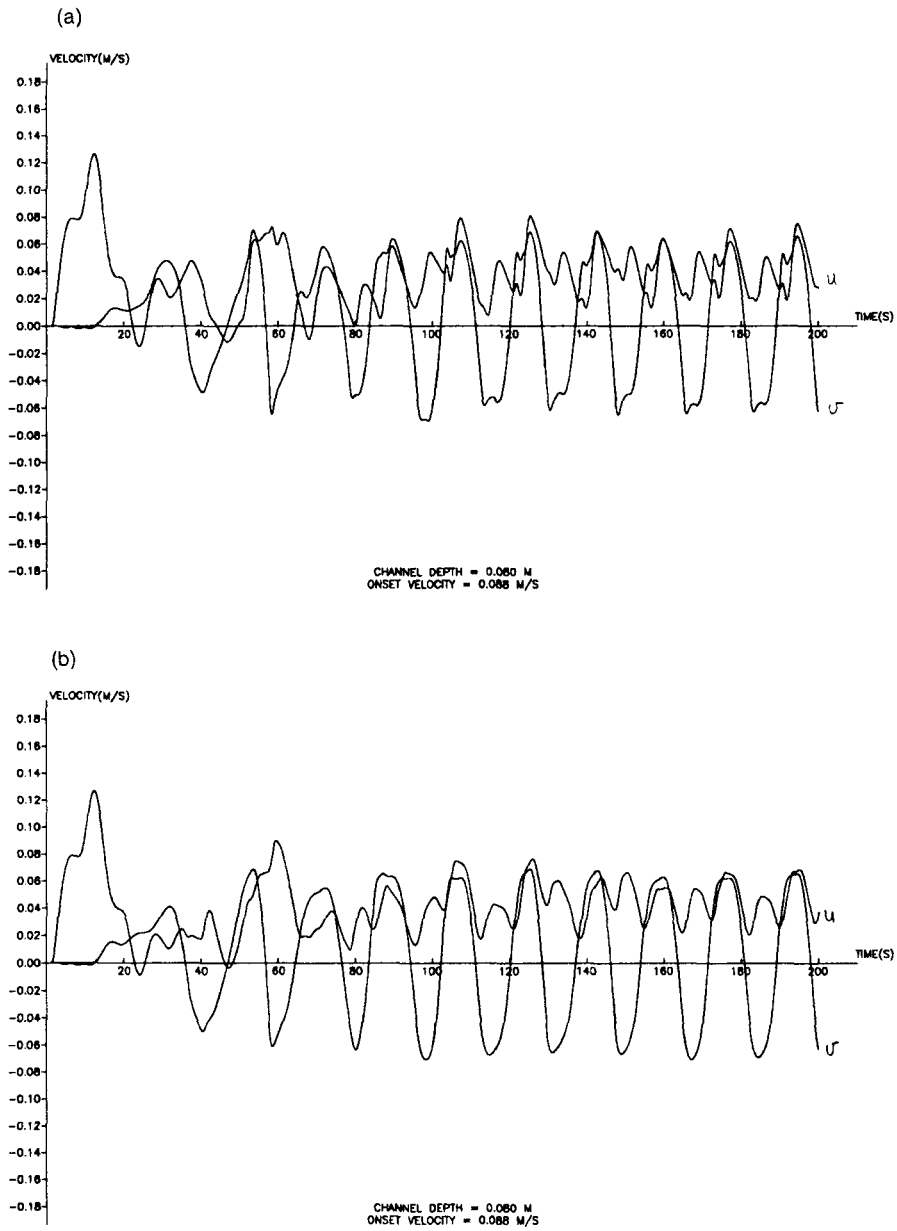

Figure 10. Variation in velocities u and v with time at $x = 1{\cdot}617$ m, $y = 0{\cdot}726$ m from 3D computation: (a) surface cell; (b) mid-depth cell; (c) bed cell

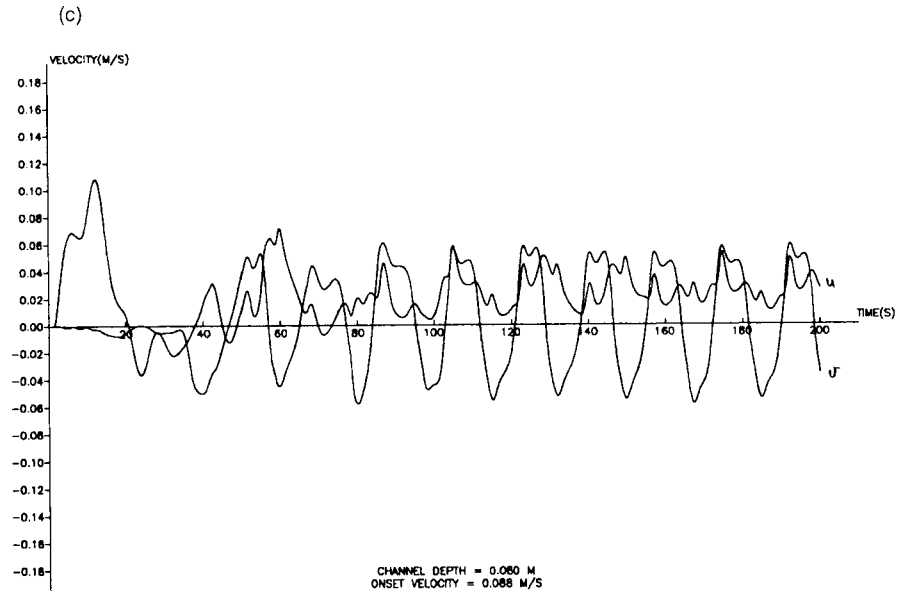

Figure 10. (Continued)

at the surface and mid-depth levels, it is at the fourth harmonic at the bed level. This has important implications for mixing processes.

Finally, it is considered worthwhile to show velocity time histories for a position close to the shoreline of the island to demonstrate the stability of the method at small depths. Figure 12 shows time histories at a distance of 0·0912 m across from the island centre ($x = 0{\cdot}76$ m, $y = 0{\cdot}669$ m; about 0·02 m from the wet/dry boundary on the lower shoulder). It can be seen that there is little variation in frequency content between bed, mid-depth and surface levels in this case.

The computations were made initially on a vector processor, the Cray EL98, which has a peak processing performance of 133 Mflops (compared with 333 Mflops for a Cray YMP, both with one processor). The 2D run for 4000 time steps on the 328 × 100 mesh required 2 h, while

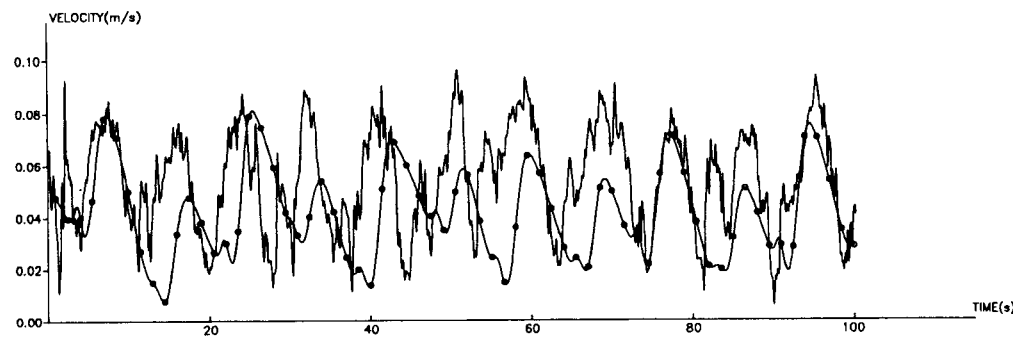

Figure 11. Variation in surface u-velocity with time from computation and LDA experimental measurement at $x = 1{\cdot}617$ m, $y = 0{\cdot}72$ m, the spiky variation being for the latter and the smooth variation for the former (with circle symbols imposed for easy identification)

the 3D run on the 328 x 100 x 20 mesh required 103 h. The 2D code vectorized almost completely. The 3D code requires several direct solutions of a tridiagonal equation set per mesh point per time step (the number of equations being equal to the number of vertical mesh spacings). Such a direct solver with back substitution involves recursion and does not vectorize. However, the scheme is well suited to parallel computing and a parallelized version of the 3D code required only 5 h 40 min for the above run on the Kendall Square Research machine with 32 processors. The specialist programming methodology is described elsewhere.[19]

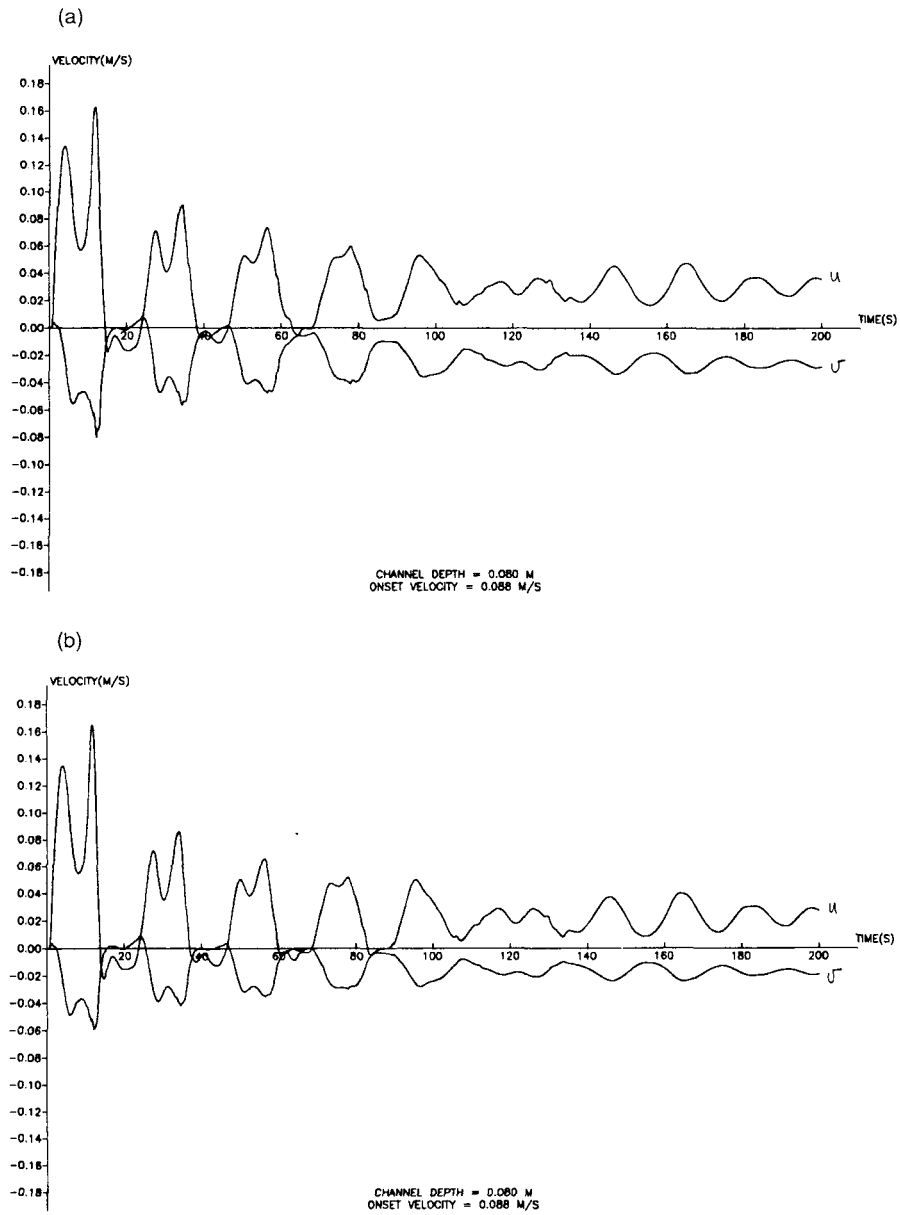

Figure 12. Variation in velocities u and v with time at $x = 0{\cdot}76$ m, $y = 0{\cdot}669$ m from 3D computation: (a) surface cell; (b) mid-depth cell; (c) bed cell

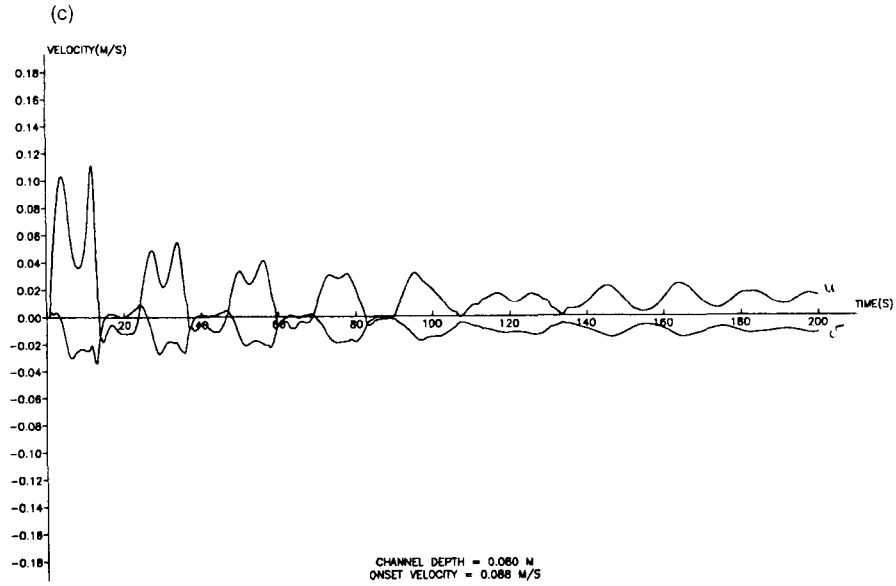

Figure 12. (Continued)

CONCLUSIONS

A semi-implicit Lagrangian form of the 3D shallow water equations has been developed to include the σ-co-ordinate transformation in the vertical direction, allowing accurate resolution of bed and surface boundary conditions. A two-layer mixing length turbulence model for the vertical direction has been incorporated. The model is for rough turbulent flow and the bed is defined only by its roughness height. The situation of vortex shedding from a conical island with gently sloping sides in a current was computed and compared with some experimental velocity measurements. The 3D computations revealed some significant 3D effects and the gross flow features showed some agreement with experiment. However, while convergence of results has been demonstrated for decreasing time step, it has not for decreasing cell size. Differences between experiment and computation require further investigation for this challenging test problem, both in relation to numerical convergence and through the use of more sophisticated turbulence modelling. Use of adaptive mesh refinement would be desirable. Effective use is being made of parallel computing.

ACKNOWLEDGEMENTS

Peter Lloyd is in receipt of an SERC Marine Technology research studentship which we gratefully acknowledge. The LDA measurements were made with the generous assistance of Dr. John Turner, Victor Chan and Derek Robinson in Mechanical Engineering. The assistance of Dr. Mike Pettipher from the Manchester Computing Centre on computing matters is also gratefully acknowledged.

REFERENCES

1. J. J. Leendertse, 'Aspects of a computational model for long period water wave propagation', *Memo. RM-5294-PR*, Rand Corp., Santa Monica, CA, 1967.
2. R. Garcia and R. E. Kahawita, 'Numerical solution of the St. Venant equations with the MacCormack finite-difference scheme', *Int. j. numer. methods fluids*, **6**, 259–274 (1986).

3. J. Peraire, O. C. Zienkiewicz and K. Morgan, 'Shallow water problems in a general explicit formulation', *Int. j. numer. methods eng.*, **22**, 547–574 (1986).
4. A. G. L. Borthwick and R. W. Barber, 'River and reservoir flow modelling using the transformed shallow water equations', *Int. j. numer. methods fluids*, **14**, 1193–1217 (1992).
5. B. P. Leonard, 'A stable and accurate convective modelling procedure based on quadratic upstream interpolation', *Comput. Methods Appl. Mech. Eng.*, **19**, 59–98 (1979).
6. M. A. Leschziner, 'Modelling turbulent recirculating flows by finite-volume methods—current status and future directions', *Int. J. Heat Fluid Flow*, **10**, 186–202 (1989).
7. ASCE Task Committee on Turbulence Models in Hydraulic Computations, 'Turbulence modelling of surface water flow and transport: Parts I, II, III, IV', *J. Hydraul. Eng.*, **114**, 970–1073 (1988).
8. V. Casulli, 'Semi-implicit finite difference methods for the two-dimensional shallow water equations', *J. Comput. Phys.*, **86**, 56–74 (1990).
9. A. Leonard, 'Vortex methods for flow simulation', *J. Comput. Phys.*, **37**, 289–335 (1980).
10. S. V. Patankar and D. B. Spalding, 'A calculation procedure for heat, mass and momentum transfer in three-dimensional parabolic flows', *Int. J. Heat Mass Transfer*, **15**, 1787–1806 (1972).
11. J. J. Leendertse, 'A new approach to three-dimensional free-surface flow modelling', *Rep. R-3712-NETH/RC*, Rand Corp. Santa Monica, CA, 1989.
12. *TRISULA: A Program for the Computation of Non-steady Flow and Transport Phenomena on Curvilinear Coordinates in 2 or 3 Dimensions*, Delft Hydraulics, Delft, 1993.
13. N. A. Phillips, 'A coordinate system having some special advantages for numerical forecasting', *J. Meteorol.*, **14**, 184–185 (1957).
14. V. Casulli and R. T. Cheng, 'Semi-implicit finite-difference methods for three dimensional shallow water flow', *Int. j. numer. methods fluids*, **15**, 629–648 (1992).
15. W. Rodi, *Turbulence Models and Their Applications in Hydraulics*, 2nd edn, IAHR, 1984.
16. P. K. Stansby and A. Slaouti, 'Simulation of vortex shedding including blockage by the random-vortex and other methods', *Int. j. numer. methods fluids*, **17**, 1003–1013 (1993).
17. P. M. Lloyd and P. K. Stansby, 'Unsteady surface-velocity field measurement using video analysis', *Proc. IAHR Symp. on Waves—Physical and Numerical Modelling*, Vancouver, 1994.
18. R. Booij, 'Depth-averaged k–ε modelling', *Proc. IAHR Congr.*, Ottawa, 1989, pp. A199–A206.
19. C. Falco Korn, J. M. Bull, G. D. Riley and P. K. Stansby, 'Effective use of parallel processing for 3-D shallow-water flow', *Sci. Prog.*, in press.